Journal of Sol-Gel Science and Technology (2022) 104:526–535
https://doi.org/10.1007/s10971-022-05843-8

INVITED PAPER: NANO- AND MACROPOROUS MATERIALS (AEROGELS, XEROGELS, CRYOGELS, ETC.)

Mechanical and thermal properties of porous polyimide monoliths crosslinked with aromatic and aliphatic triamines

Mitsuhiro Ishida[1] · Yutaro Sashiyama[2] · Hirofumi Akamatsu[2] · Katsuro Hayashi[2] · Kazuki Nakanishi[1] · George Hasegawa[1]

Received: 23 March 2022 / Accepted: 10 May 2022 / Published online: 20 May 2022

Abstract

Thermal insulating materials are of importance for efficient and effective use of heat energy. Porous organic foams are widely employed for this purpose owing to their low thermal conductivity and mass productivity at low cost. However, the poor thermal stability of organic polymers limits their availability within a low temperature range (typically, < 150 °C). In this paper, we demonstrate the one-pot sol–gel synthesis of porous poly(amic acid) (PAA) xerogels and their conversion to porous polyimide (PI) monoliths by thermal imidization. The PAA networks crosslinked with either aromatic or aliphatic triamine and the bicontinuous porous morphology tailored via spinodal decomposition allow the evaporative drying at ambient pressure to obtain low-density PAA xerogels without significant shrinkage. The aromatic crosslinker yields the porous PI monoliths with higher porosity and flexible feature as compared with those prepared with the aliphatic triamine. On the other hand, the porous PI monolith based on the aliphatic crosslinker possesses slightly higher thermal stability owing to the stiffer mechanical property. The durability test results verify the porous PI thermal insulators are available in air at up to ~450 °C for a short period and up to ~350 °C for a long term.

Graphical abstract

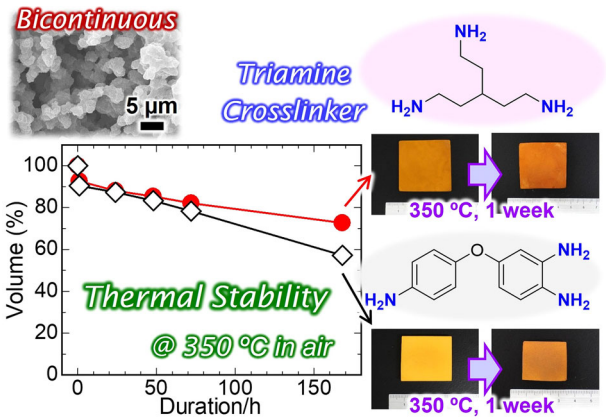

Supplementary information The online version contains supplementary material available at https://doi.org/10.1007/s10971-022-05843-8.

✉ George Hasegawa
h-george@imass.nagoya-u.ac.jp

[1] Institute of Materials and Systems for Sustainability, Nagoya University, Furo-cho, Chikusa-ku, Nagoya 464-8601, Japan

[2] Department of Applied Chemistry, Graduate School of Engineering, Kyushu University, Motooka, Nishi-ku, Fukuoka 819-0395, Japan

Keywords Poly(amic acid) xerogels · Phase separation · Imidization · Thermal conductivity · Thermal stability

Highlights

- Porous poly(amic acid) xerogels with bicontinuous morphology are fabricated via the phase separation method.
- Crosslinked polymer networks are synthesized by using either aromatic or aliphatic triamine crosslinker.
- Porous polyimide monoliths prepared with the aromatic crosslinker show the lower shrinkage during thermal imidization.
- The polyimide network crosslinked with the aliphatic triamine exhibits the higher thermal stability against shrinkage.
- The long-term durability test reveals the availability of the polyimide thermal insulators at up to 350 °C in air.

1 Introduction

Toward the achievement of a sustainable society, thermal control in various situations is of great importance for saving energy. In particular, thermal insulating can reduce loss of heat energy to ambient and thereby energy consumption. In general, highly porous materials show low thermal conductivity owing to small contribution of heat transfer through solid, which is much faster than that through gases (air) [1]. In this context, aerogels with extremely high porosity are the most promising materials as a thermal insulator. Indeed, the nanoporous aerogels have excellent thermal insulating capability with fairly low thermal conductivity (<20 mW m^{-1} K^{-1}) [1, 2], which is even lower than that of air (~26.4 mW m^{-1} K^{-1} at 27 °C) [3] by virtue of suppressing the heat conduction by gas molecules within confined spaces smaller than their mean free paths [1, 4]. Recently, rising attention have been given to the aerogels derived from organic polymers in view of their lower thermal conductivity in solid and higher mechanical stability as compared to the inorganic counterparts. For example, the conductivity of only 13 mW m^{-1} K^{-1} was reported for the first developed organic aerogel [5]. However, there is a significant shortcoming for organic aerogels, which is the low thermal stability; most of organic polymers are pyrolyzed above ~200 °C in air, which limits their usage to the low temperature range.

Polyimide (PI) shows exceptionally high thermal stability among the organic polymers, which extends the applicable temperature range of organic aerogel insulators up to ~500 °C [6, 7]. Therefore, a great deal of effort has been devoted to developing PI aerogels to date [8–25]. Nevertheless, the practical use of PI aerogels is still challenging because of the high production cost and the limitation of producible size dominated by the size of a compression chamber for supercritical drying [26, 27]. Hence, it is desirable to develop a synthetic pathway of porous PI monoliths without any special drying processes. To this end, rational design for the crosslinked polymer networks as well as the porous morphology is required so as to minimize the shrinkage due to surface tension during evaporative drying at ambient pressure.

Linear PI chains are prepared via the imidization of poly (amic acid) (PAA) precursors which are synthesized by the polymerization between dianhydrides and diamines. In order to obtain three-dimensionally (3D) crosslinked PI networks, amine-based crosslinkers bearing three or more functional groups for hyperbranching is required [7, 28]. Alternatively, triisocyanates [15, 21] and tricarbonyl chlorides [17, 20, 21] can be utilized as well, though they need careful handling due to the high reactivity. Regarding the porous morphology with mechanical robustness for suppressing shrinkage during evaporative drying, 3D interconnected macropore frameworks are beneficial [29]. The preceding studies have revealed that various crosslinked polymer resins with such macroporous structures can be fabricated by the phase separation method, where the so-called bicontinuous morphology formed on the course of spinodal decomposition is fixed by gelation in the individual polymerizing systems [29–35].

In this study, we have prepared porous PI monoliths with bicontinuous morphology aiming at developing thermal insulators usable in a relatively high temperature range. The porous PAA precursors were fabricated using either aromatic or aliphatic triamine crosslinker via the phase separation strategy and the evaporative drying process. The PAA and PI samples derived from the different crosslinkers were compared in terms of the gelation and imidization behavior, pore property, mechanical strength, and thermal conductivity as well as stability. The findings obtained by the present study provide a guideline for producing porous PI monoliths and disclose their applicability as a thermal insulator at elevated temperatures in air.

2 Experimental procedure

2.1 Chemicals

Pyromellitic dianhydride (PMDA), 4,4'-oxydianiline (ODA), 3,4,4'-triaminodiphenyl ether (TADPE) and tris(2-aminoethyl)amine (TAEA) were purchased from Tokyo Chemical Industry Co., Ltd. Poly(ethylene oxide) (PEO, $M_W = 1\,000\,000$) and *N*,*N*-dimethylacetamide (DMA) were obtained from Sigma-Aldrich Co. and Kishida Chemical Co., Ltd., respectively. All reagents were used as received.

2.2 Sample preparation

The molar ratio of [PMDA]:[ODA]:[TADPE or TAEA] was set as 1:1–3x/2:x, premising the ideal reaction between an acid anhydride and an amino group to yield a poly(amic acid) (PAA) network. The starting compositions of the samples prepared in this study are listed in Table 1. In a typical synthesis, the acid anhydride (PMDA), the amines (ODA & TADPE or ODA & TAEA) and the phase separation inducer (PEO) were dissolved in DMA at 120 °C, respectively, to obtain three solutions (one-third of the total volume of DMA was added to each solution). Then, the solution of PMDA was added to that of PEO, followed by adding the solution of amines. Thus obtained homogeneous solution was subsequently kept at 120 °C for 24 h for gelation and aging. Note that, in the case with the TADPE crosslinker, the mixed sol soon underwent gelation once, and gradually turn to sol again. The second gelation gave rise to a crosslinked gel. The wet gels were washed with 2-propanol and dried at 60 °C to obtain the PAA xerogels. The imidization of PAA xerogels was performed by the thermal treatment at 300 °C for 2 h in air (heating rate: 5 °C min^{-1}).

2.3 Characterization

Microscopic observation of the samples was conducted with a scanning electron microscope (SEM; JSM-6060S, JEOL). The thermogravimetry (TG) and differential thermal analysis (DTA) measurements were performed by Thermo plus TG 8120 (Rigaku Corp.) at a heating rate of 5 °C min^{-1} while continuously supplying air at a rate of 100 mL min^{-1}. The Fourier-transform infrared (FT-IR) spectra of the samples were obtained using an FT-IR spectrometer equipped with an attenuated total reflectance (ATR) module with a diamond prism as the waveguide (IRTracer-100, Shimadzu Co., Japan). Wide-angle X-ray scattering (WAXS) measurements were carried out for the ground samples on an X-ray diffractometer (Aeris; Malvern Panalytical Ltd.) using Cu Kα radiation ($\lambda = 1.5404$ Å). N_2 sorption measurements (Belsorp mini II, Bel Japan Inc.) were performed at 77 K to investigate the micro- and mesoporous properties. The PAA and PI samples were degassed under vacuum at 100 and 200 °C, respectively, before the measurements. Uniaxial compression tests were carried out on the porous PI monoliths with a material tester (EZGraph, Shimadzu Corp.), while thermal conductivity was measured under ambient pressure with a transient heat flow meter (HFM 446 Lambda Small, Netzsch GmbH). As regards the thermal durability tests, the porous PI monoliths were held in an electric furnace under air atmosphere at varied temperatures for different duration, and the weight and dimension of the heat-treated samples were recorded.

3 Results and discussion

The monomer reagents to synthesize crosslinked PAA networks in this study are displayed in Fig. 1. The polycondensation of PMDA and ODA yields a linear PAA polymer, which is a common precursor of PI. The substitution of aromatic (TADPE) [28] or aliphatic triamine (TAEA) [23, 24] for ODA provides a three-dimensionally (3D) crosslinked network. It was found that gelation did not occur with the thorough substitution while the relatively low substitution ratios tended to give a rigid gel in both triamine systems.

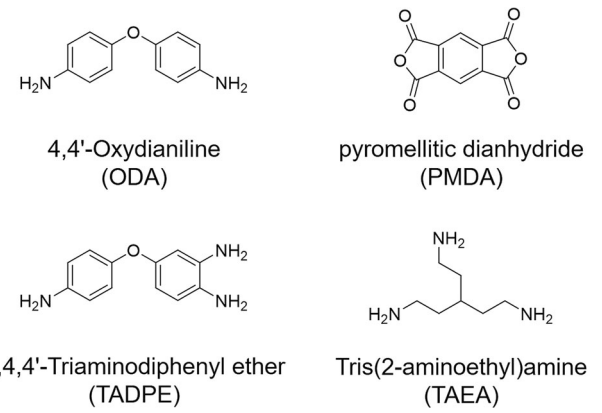

Fig. 1 Chemical structures of the monomer species to obtain crosslinked PAA networks

Table 1 Starting compositions of the samples

	PMDA/mmol	ODA/mmol	TADPE/mmol	TAEA/mmol	PEO/mg	DMA/mL
TADPE-crosslinked sample (DMA-4.8 mL)[a]	3.0	2.25	0.50	–	0–42	4.8
TADPE-crosslinked sample (DMA-9.0 mL)[b]	3.0	1.95	0.70	–	42–54	9.0
TAEA-crosslinked sample (DMA-9.0 mL)[c]	3.0	2.33	–	0.45	24–84	9.0

The molar ratio of [PMDA]:[ODA]:[TADPE or TAEA] was set as 1:1–3x/2:x, while the amount of PEO was varied

[a] $x = 0.167$

[b] $x = 0.233$

[c] $x = 0.15$

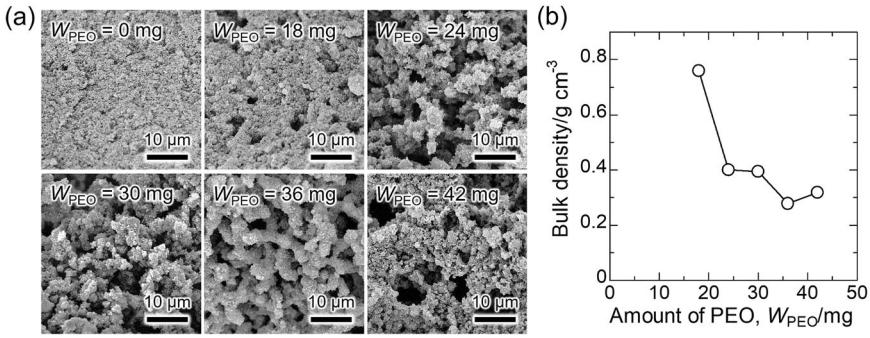

Fig. 2 Variation of (**a**) macroporous morphology and (**b**) bulk density for the TADPE-crosslinked PAA xerogels ($x = 0.167$; 4.8 mL of DMA) prepared with varied amounts of PEO (W_{PEO})

3.1 Porous PAA xerogels with TADPE crosslinker

Figure 2a shows the microscopic morphologies of the samples prepared with the molar ratio of PMDA:ODA:TADPE = 1:0.75:0.167 ($x = 0.167$). Without addition of PEO, the wet gel was subjected to the large shrinkage during drying, resulting in the xerogels with no macroporous structure. On the other hand, the wet gels with PEO had an opaque and brown appearance as a result of phase separation. The bicontinuous macroporous morphologies were observed in the samples with $W_{PEO} = 24$–36 mg. As verified in Fig. 2b, the bulk density took the minimum value of 0.28 g cm^{-3} at $W_{PEO} = 36$ mg, where the volumetric shrinkage during drying was *ca*. 39%.

This result indicates that PEO ($M_W = 1\ 000\ 000$) can induce the spinodal decomposition in this sol–gel system of PAA [30–35]. It should be mentioned that PEO with the smaller molecular weight ($M_W = 100\ 000$) also evoked phase separation while the resultant samples showed no clear bicontinuous structure but particle aggregate-like morphology (see Fig. S1). The similar tendency where PEO with the higher molecular weight is more effective to induce spinodal decomposition forming the bicontinuous morphology was found in the methacrylate-based gels prepared by the controlled/living radical polymerization [34].

For the purpose of obtaining PAA xerogels with enhanced porosity, the samples were prepared with increased volume of solvent. When the volume of DMA was increased from 4.8 mL to 9.0 mL, the gelation time was prolonged from ~120 min to ~300 min. In the diluted system, it was found that the monomer molar ratio of PMDA:ODA:TADPE = 1:0.65:0.233 ($x = 0.233$) was favorable for preparing the porous xerogel with suppressed shrinkage during drying. Figure 3 shows the macroporous structures of the PAA xerogels bearing the bicontinuous structures. The appearance of the representative sample is also given. The macroporous structure became coarser as the amount of PEO increased. The volumetric shrinkage during drying was estimated as 51–54%, while the bulk density was reduced down to 0.21 g cm^{-3} at $W_{PEO} = 48$ mg.

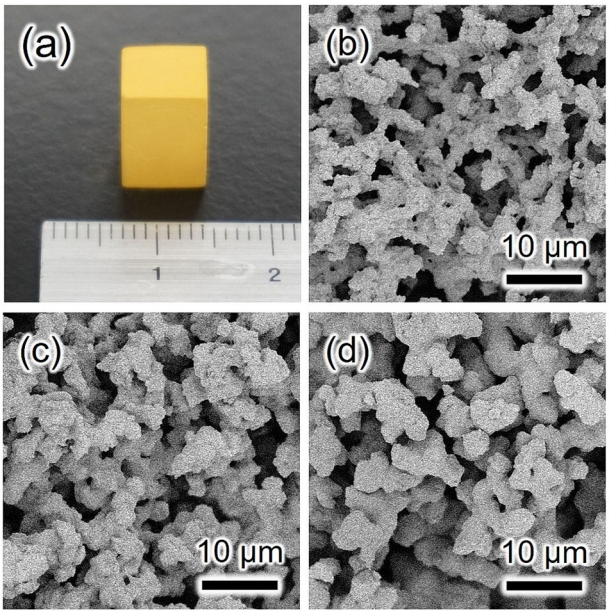

Fig. 3 **a** Appearance and (**b**–**d**) bicontinuous structures of the TADPE-crosslinked PAA xerogels ($x = 0.233$; 9.0 mL of DMA) prepared with varied amounts of PEO: **b** $W_{PEO} = 42$ mg, **c** $W_{PEO} = 48$ mg, **d** $W_{PEO} = 54$ mg

3.2 Porous PAA xerogels with TAEA crosslinker

As with the investigation of PAA prepared with TADPE, the relationship between the starting composition and the microscopic morphology was explored in the case of TAEA. The samples were synthesized with the fixed amount of PEO ($W_{PEO} = 60$ mg) and DMA (9.0 mL) while the amount of the crosslinker (x) was varied (Fig. S2). Similarly to the abovementioned PAA prepared with TADPE, the relatively small amounts of TAEA are favorable for obtaining porous xerogels. It should be noted that the sol with $x = 0.20$–0.40 formed precipitates prior to gelation resulting in the heterogeneous gels. The amount of precipitates was found to increase as that of TAEA was increased. On the other hand, the TAEA amount of $x = 0.05$–0.15 allowed for the homogeneous gelation. As shown in Fig. S2, the addition of PEO can bring about the phase

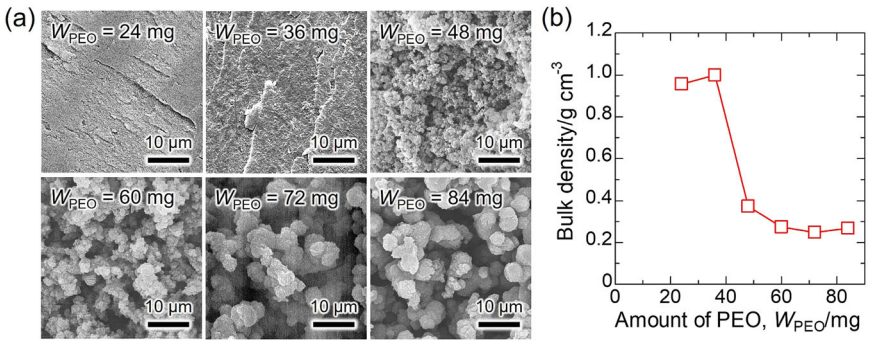

Fig. 4 Variation of (**a**) macroporous morphology and (**b**) bulk density for the TAEA-crosslinked PAA xerogels ($x = 0.15$; 9.0 mL of DMA) prepared with varied amounts of PEO (W_{PEO})

separation in the sol–gel system and the xerogels with bicontinuous morphology were obtained. It is worth mentioning that the gelation time became longer with increasing the amount of TAEA: ~280 min ($x = 0.05$), ~320 min ($x = 0.10$), and ~360 min ($x = 0.15$). Meanwhile, the PAA xerogel prepared with $x = 0.05$ had the low bulk density of 0.16 g cm^{-3} owing to the small volumetric shrinkage during drying (*ca.* 22%), while the samples with $x = 0.10$ and 0.15 showed the larger shrinkage of 51 and 60%, respectively, resulting in the higher bulk density (0.26 g cm^{-3} and 0.27 g cm^{-3}). However, the PAA xerogel prepared with $x = 0.05$ was very brittle and hardly shaped into a specific form. Accordingly, it was revealed that the TAEA amount of $x = 0.10$–0.15 is suitable to prepare porous PAA gels.

The morphological variation of the PAA xerogels ($x = 0.15$) with varied amounts of PEO are shown in Fig. 4a. The bulk density values of the samples are plotted as a funtion of the amount of PEO (W_{PEO}) in Fig. 4b. Similarly to the TADPE-based system described above, the PAA xerogels with bicontinuous macroporous structure were obtained when W_{PEO} was 48 mg and 60 mg. The xerogels prepared with the smaller amounts of PEO ($W_{PEO} = 24$–36 mg) incurred remarkably large shrinkage (~90% in volume) resulting in the dense samples with no macroporosity, whereas those with the larger amounts ($W_{PEO} = 72$–84 mg) showed the particle aggregate morphology. These samples has the bulk density similar to the PAA xerogels with bicontinuous structure, but more fragile mechanical property.

3.3 Conversion to porous PI monoliths

Hereinafter, we focus on the representative specimen with bicontinuous structure for each system. The imidization of PAA into PI is allowed by either chemical converstion or thermal treatment [36–38]. In this study, the latter pathway was employed for imidization; the PAA xerogels were simply heated in air. Figure 5a shows the TG-DTA curves of the PAA xerogels prepared with TADPE and TAEA crosslinkers. The profile of the TADPE-crosslinked sample shows the weight loss (*ca.* 6.8 wt.%) around 300 °C along with a small exothermic signal, which is indicative of the imidization along with crystallization [39]. The sharp weight loss together with a clear exothermic peak around 600 °C is attributable to the combustion of the sample. Concerning the TAEA-crosslinked sample, the weight loss arising from the imidization is observed in the temperature range similar to the TADPE-crosslinked sample. However, it appears that the weight loss overlaps with the gradual weight decrease. It indicates that the TAEA-crosslinked PAA network was subjected to the thermal degradation before the combustion starting at ~500 °C. It is speculated that aliphatic portions in the TAEA-crosslinked networks, which are more susceptible to the oxidative reaction than the aromatic moieties, are responsible for the gradual weight loss. Difference of thermal stability depending on the triamine crosslinker is to be discussed in more detail hereinafter.

Based on the TG-DTA results, the thermal imidization was performed at 300 °C in this study so as to minimize damage on the PI networks. In both samples, the color turn darker after the thermal treatment. Figure 5b demonstrates the FT-IR spectra of the samples before and after the thermal treatment. In both cases, the as-dried and heated samples exhibited the similar profiles: the characteristic absorption bands indexed to the imide ring, *e.g.* 1774 cm^{-1} (C=O in-phase stretching), 1375 cm^{-1} (C–N stretching) and 723 cm^{-1} (C=O bending) can be detected even in the spectra of as-dried samples [40, 41]. It indicates that the partial imidization took place during aging in DMA solvent at 120 °C [36]. This is compatible with the TG result that the weight loss for the imidization in the TADPE-crosslinked sample was smaller than the calculated value based on the premise of full conversion from PAA to PI in the PMDA and ODA system (8.6 wt.%). The small absorption bands at 1624 cm^{-1} and 1545 cm^{-1}, which are attributed to the C=O stretch and CNH bend-stretch of the amide linkage, respectively [40, 41], disappeared in the spectra of heat-treated samples. This change in the FT-IR profile confirms that the thermal treatment allowed for the conversion to PI.

Variation of the xerogels during thermal imidization was also pursued by WAXS (Fig. 5c). It is noteworthy that not only the heat-treated samples but also the as-dried xerogels

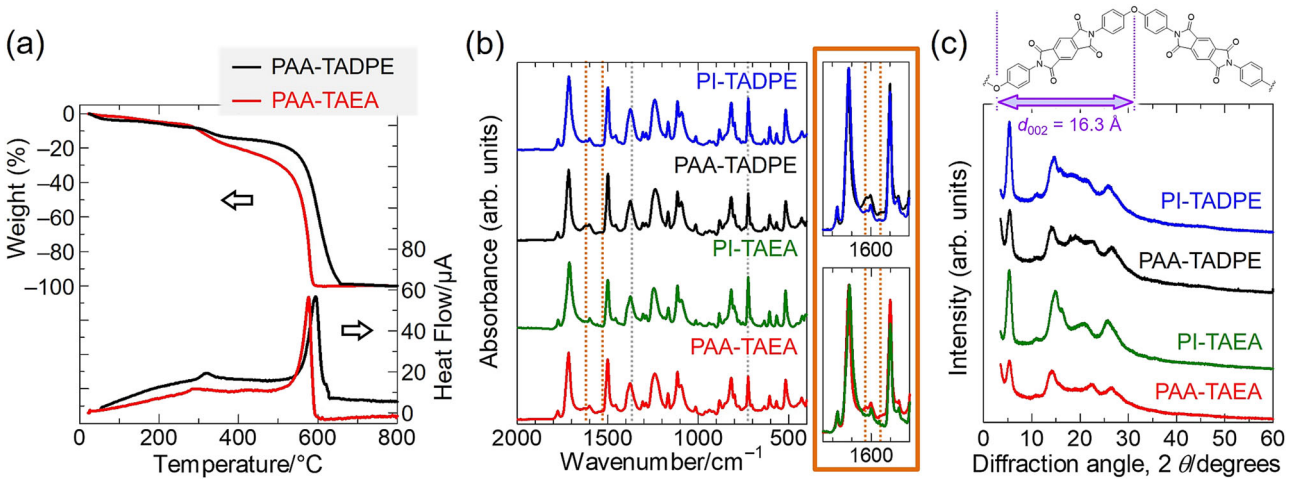

Fig. 5 **a** TG-DTA profiles in air for the TADPE- and TAEA-crosslinked PAA xerogels. **b** FT-IR spectra. **c** XRD patterns of the porous PAA and PI monoliths prepared with TADPE and TAEA crosslinkers. The magnified FT-IR profiles are also given in (**b**), where the orange broken lines denote the signals stemming from the amide linkage in PAA networks (C=O stretch at 1624 cm^{-1} and CNH bend-stretch at 1545 cm^{-1}). The illustration in (**c**) signifies the repeat unit of the PMDA-ODA polyimide corresponding to the XRD peak at 5.4 °

exhibited the crystalline scattering in both TADPE- and TAEA-based systems. Although not identical, all the WAXS profiles are reminiscent of that of the crystalline PMDA-ODA polyimide [42–46]. The diffraction peak at 5.4 ° corresponding to the *d* spacing of 16.3 Å is attributed to the repeat unit along the molecular chain of the pseudo-orthorhombic PMDA-ODA polyimide (002 reflection). The bumps positioned at ~14 °, ~22 ° and 26 ° are indexed to the 101, 010 and 111 reflections, respectively [45, 46]. This result is in good agreement with the FT-IR spectra in Fig. 5b implying the presence of imide groups in the as-dried samples. The diffraction intensity was augmented by the thermal treatment in both cases, confirming the increase of crystallinity. In addition, though the peak position of the 002 reflection remained unchanged, the peak shifts were observed for the other reflections in the heat-treated samples, which indicates the slight change of the lateral chain packing.

The thermal imidization of the PAA xerogels was accompanied by the shrinkage, resulting in the increase of bulk density (see Table 2). The TAEA-crosslinked specimens were inclined to undergo larger shrinkage (volumetric shrinkage of ~38%) by the thermal treatment at 300 °C compared with the TADPE-crosslinked xerogels (~27%). Consequently, the bulk density of the TAEA-crosslinked monolith was 0.39 g cm^{-3}, whereas that of the TADPE-crosslinked sample was kept as low as 0.24 g cm^{-3}. In both cases, however, the crack-free monolithic appearance as well as the bicontinuous macroporous morphology remained almost unchanged as signified in Fig. 6a, b. On the other hand, as manifested by the N_2 physisorption results (Fig. 6c, d), the smaller pores residing in the macropore framework of the PAA xerogels were considerably decreased by the heat treatment in both TADPE- and TAEA-crosslinked samples. As a result, the specific surface area dropped from 140–160 to 12–14 m^2 g^{-1}.

Table 2 Pore properties of the samples calcined at different temperatures

	S_{BET} [a]/m^2 g^{-1}	V_p [b]/cm^3 g^{-1}	ρ_{bulk} [c]/g cm^{-3}	Porosity[d]/%
PAA-TADPE	140	0.33	0.21	85
PI-TADPE	12	0.056	0.24	83
PAA-TAEA	160	0.37	0.27	81
PI-TAEA	14	0.034	0.39	73

The TADPE-crosslinked samples (PAA-TADPE and PI-TADPE) were prepared with the starting composition of DMA-9.0 mL, $x = 0.233$ and $W_{PEO} = 48$ mg, while the TAEA-crosslinked samples (PAA-TAEA and PI-TAEA) were prepared with that of DMA-9.0 mL, $x = 0.15$ and $W_{PEO} = 60$ mg

[a]Specific surface area obtained by the BET method

[b]Micro- and mesopore volume obtained by N_2 adsorption isotherms at $p/p_0 = 0.99$

[c]Bulk density calculated as [weight]/[bulk volume]

[d]Calculated as 100 × (1–[bulk density]/[true density])

3.4 Mechanical and thermal properties of porous PI monoliths

The mechanical properties of the porous PI monoliths were investigated by the uniaxial compression test, and the stress-strain curves are shown in Fig. 7a. The TAEA-crosslinked PI monolith showed the relatively stiff nature with the Young's modulus of 34 MPa, being fractured at < 5% strain. By contrast, the TADPE-crosslinked PI monolith showed more flexible behavior; although some small cracks formed, the monolith was compressible to 30% strain (Fig.

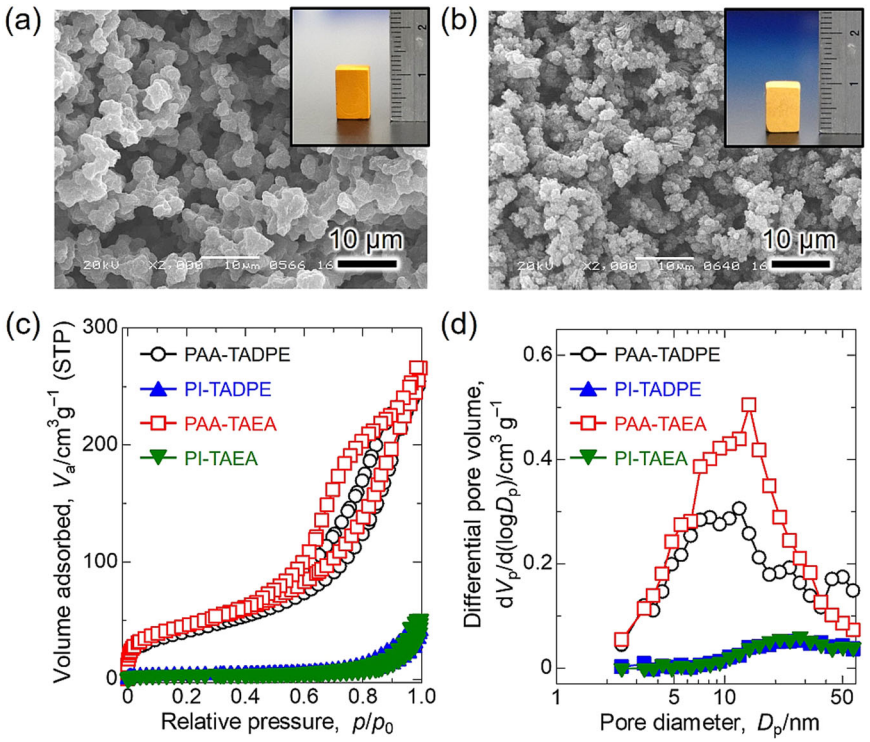

Fig. 6 **a**, **b** Appearances (inset) and SEM images of the porous PI monoliths prepared with (**a**) TADPE and (**b**) TAEA. **c** N_2 adsorption-desorption isotherms and (**d**) the correspondent mesopore size distributions obtained by the BJH method for the porous PAA and PI monoliths prepared with TADPE and TAEA crosslinkers

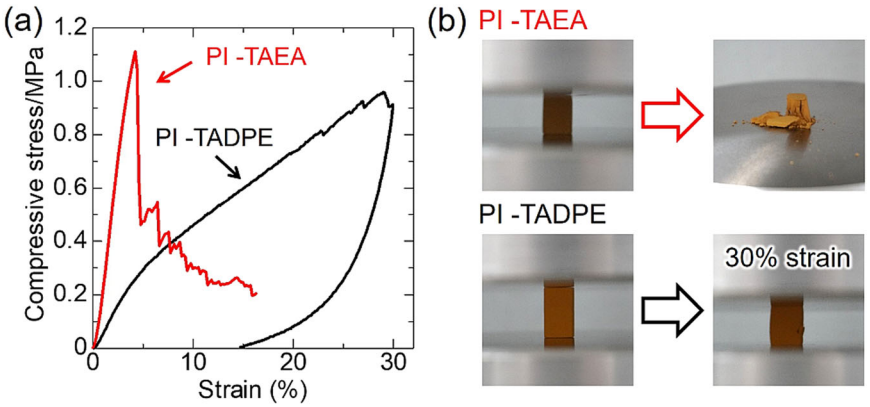

Fig. 7 **a** Representative stress-strain curves upon uniaxial pressing of the TADPE- and TAEA-crosslinked PI monoliths. **b** Digital images showing the difference in compressive behavior between the TADPE- and TAEA-crosslinked PI monoliths

7b). After removing the compressive stress, the monolith was recorvered to some extent, leaving the residual strain of ~8.5%. The Young's modulus was estimated as 7.7 MPa for the TADPE-crosslinked sample.

The thermal conductivity of the porous PI monoliths was measured by means of the heat flow method combining twelve PI panels (Fig. 8a). The thermal conductivity at room temperature (25 °C) was evaluated as 46 mW m^{-1} K^{-1} and 52 mW m^{-1} K^{-1} for the TADPE- and TAEA-crosslinked PI monoliths, respectively. These values are on par with those of the commercial organic insulators like polyurethane and polystyrene foams (typically, 40–50 mW m^{-1} K^{-1} at 25 °C) [25]. Figure 8b exhibits the temperature dependence of thermal conductivity. For both samples, the thermal conductivity shows a linear relationship with the temperature. The increase rate was slightly higher for the TADPE-crosslinked monolith, which however showed the lower conductivity and thereby the better heat insulating capability in the measured temperature range (0–70 °C). This is probably because of the lower bulk density for the TADPE-crosslinked sample (Table 2).

For the purpose of corroborating the thermal stability of the PI monoliths, the degradation upon heating in air was examined in terms of the change in bulk density and the volumetric shrinkage. Each porous PI sample was exposed to the heat-treatment in air at 350, 400, 450 and 480 °C with the duration of 1 h in sequence. The results are summarized in Fig. 8c. As already mentioned, the TAEA-crosslinked PAA xerogel shrank to the greater extent by the thermal imidization, resulting in the large increase of bulk density. On the other hand, the volume change ratio upon the heat-treatment was

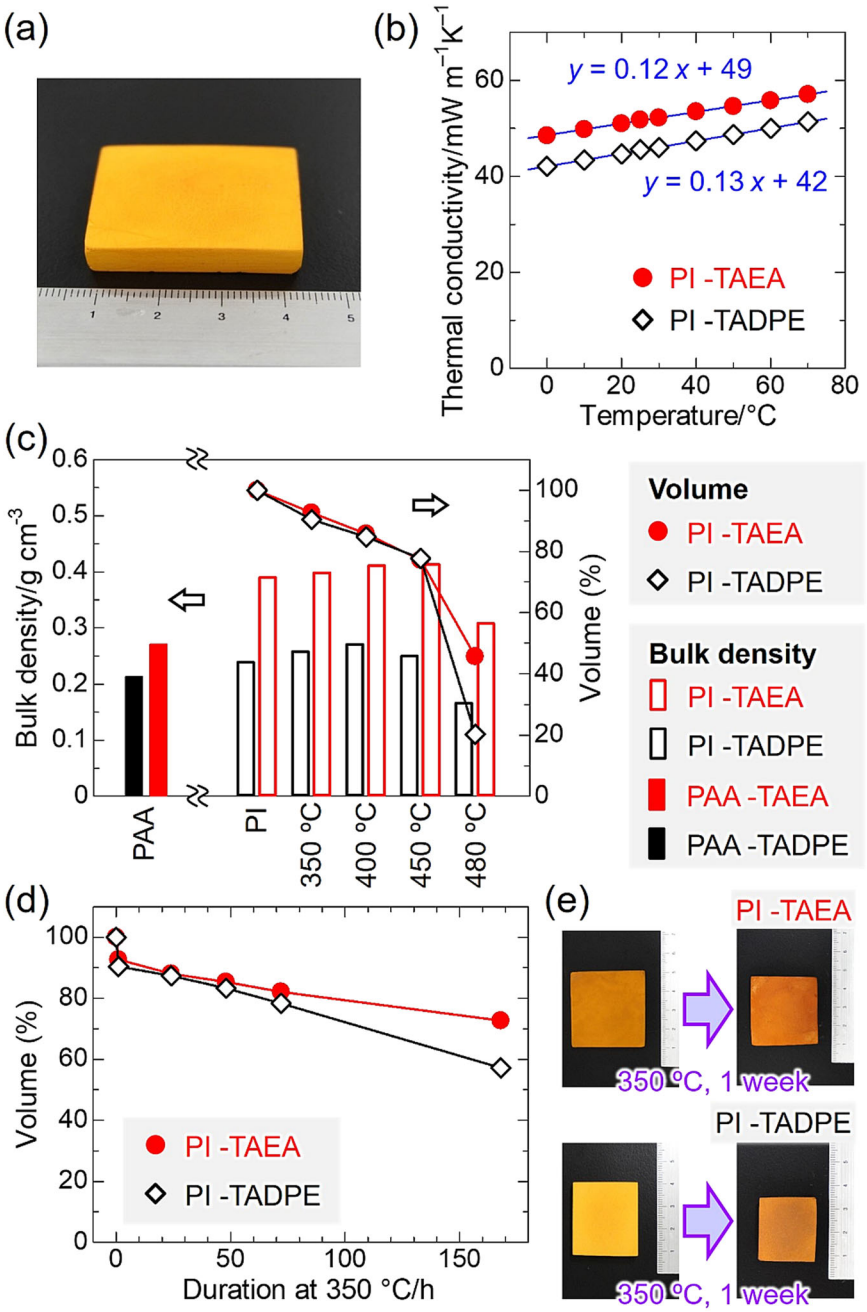

Fig. 8 **a** Appearance of the porous PI panel for the thermal conductivity test. **b** Thermal conductivity values plotted as a function of temperature for the porous PI monoliths. The lines are drawn by the least-squares method. **c** Variation of bulk density and volume by the heat-treatment at elevated temperatures for 1 h in air for the TADPE- and TAEA-crosslinked samples. **d** Volume change in heating at 350 °C in air for the TADPE- and TAEA-crosslinked samples. **e** Digital images of the TADPE- and TAEA-crosslinked PI monoliths before and after the durability test (350 °C; 168 h)

found to be almost the same for the two PI samples up to 450 °C. The porous PI monoliths shrank simultaneously with the weight decrease to the similar extent, resulting in the small change in bulk density. The clear degradation was observed for the PI monoliths after the heat-treatment at 480 °C. The samples considerably shrank associated with the color change to dark brown. In addition, the sample weight was also dramatically decreased to ~14 and ~36%, for the TADPE- and TAEA-crosslinked monoliths, respectively. In this sence, the pyrolysis took place more slowly on the TAEA-crosslinked sample. Both samples were completely burnt out after heat-treatment at 500 °C for 1 h.

The durability of the porous PI monoliths was also explored by the long-term duration test. Both PI monoliths were completely spoiled with the large weight loss after the treatment at 450 °C for 6 h. When holding the samples at 400 °C, 62 and 31% of volume shrinakge were detected after 24 h for the TADPE- and TAEA-crosslinked PI monoliths, respectively. The volume change of the porous PI monoliths in heating at 350 °C as a function of duration time is plotted in Fig. 8d. As is the case with the short-term stability test (Fig. 8c), the volume change ratios were similar to the weight change, and therefore, the bulk density remained almost constant for both porous PI monoliths.

Both samples continuously shrank with time, while the larger shrinkage was imposed on the TADPE-crosslinked PI monolith; the TAEA-crosslinked sample exhibited higher durability with *ca*. 27% volume shrinkage after heating at 350 °C for 168 h (see also Fig. 8e). It is deduced that the stiffer mechanical property with higher Young's modulus, as shown in Fig. 7a, accounts for the suppressed shrinkage for the TAEA-crosslinked PI monolith.

4 Conclusion

Porous PAA xerogels with bicontinuous morphology have been successfully fabricated by the sol–gel process accompanied by phase separation. Two triamine crosslinkers, aromatic TADPE and aliphatic TAEA, were employed to form robust 3D-crosslinked polymer networks that allow the evaporative drying at ambient pressure. In both cases, the relatively small amount of triamine was found to be favorable for homogeneous gelation as well as suppression of shrinkage during drying, and the addition of PEO induced the spinodal decomposition giving rise to the 3D-interconnected macroporous structures. The macropore skeletons involved well-defined mesopores, resulting in the hierarchically porous PAA xerogels. It was also revealed that both TADPE- and TAEA-crosslinked PAA networks were partially crystallized to PI during the aging process at 120 °C.

The thermal imidization of the PAA xerogels provided the porous PI monoliths with preserved macroporous structure and enhanced crystallinity. On the other hand, the skeletal pores were largely decreased due to the shrinkage. The TAEA-crosslinked sample was subjected to the larger shrinkage than the TADPE-crosslinked counterpart. The TAEA-crosslinked PI monolith showed the stiffer mechanical property being fractured by the small uniaxial deformation, whereas the TADPE-crosslinked sample exhibited more flexible behavior against compression. Concerning the thermal properties, the TADPE-crosslinked PI monolith was imbued with the better thermal insulating capability owing to the lower bulk density and thereby higher porosity, while the TAEA-crosslinked one exhibited slightly higher thermal stability in air presumably because of the stiffer mechanical property. The thermal stability tests verified that the porous PI monoliths can be used as a thermal insulator at up to 350 °C in air considering the long-term duration, though they withstood the treatment at 450 °C for a short period (~1 h).

Acknowledgements This work was supported by the Asahi Glass Foundation. Financial supports from Japan Science and Technology Agency (JST) FOREST Program (Grant Number JPMJFR2021, Japan) is also acknowledged.

Author contributions MI and YS contributed equally to the sample preparation and the data collection. HA, KH and KK took part in discussion on the data analyses. GH designed the study, collected the data and wrote the first draft of this manuscript. All authors read and approved the final manuscript.

Compliance with ethical standards

Conflict of interest The authors declare no competing interests.

Publisher's note Springer Nature remains neutral with regard to jurisdictional claims in published maps and institutional affiliations.

References

1. Fricke J (1988) Aerogels – highly tenuous solids with fascinating properties. J Non-Cryst Solids 100:169–173. https://doi.org/10.1016/0022-3093(88)90014-2
2. Hüsing N, Schubert U (1998) Aerogels – airy materials: Chemistry, structure, and properties. Angew Chem Int Ed 37:22–45. https://doi.org/10.1002/(SICI)1521-3773(19980202)37:1/2<22::AID-ANIE22>3.0.CO;2-I
3. Lemmon EW, Jacobsen RT (2004) Viscosity and thermal conductivity equations for nitrogen, oxygen, argon, and air. Int J Thermophys 25:21–68. https://doi.org/10.1023/B:IJOT.0000022327.04529.f3
4. Hayase G, Kugimiya K, Ogawa M, Kodera Y, Kanamori K, Nakanishi K (2014) The thermal conductivity of polymethylsilsesquioxane aerogels and xerogels with varied pore size for practical application to thermal superinsulators. J Mater Chem A 2:6525–6531. https://doi.org/10.1039/C3TA15094A
5. Lu X, Arduini-Schuster MC, Kuhn J, Nilsson O, Fricke J, Pekala RW (1992) Thermal conductivity of monolithic organic aerogels. Science 255:971–972. https://doi.org/10.1126/science.255.5047.971
6. Sroog CE, Endrey AL, Abramo SV, Berr CE, Edwards WM, Olivier KL (1965) Aromatic polypyromellitimides from aromatic polyamic acids. J Polym Sci: Part A 3:1373–1390. https://doi.org/10.1002/pol.1965.100030410
7. Liaw DJ, Wang KL, Huang YC, Lee KR, Lai JY, Ha CS (2012) Advanced polyimide materials: syntheses, physical properties and applications. Prog Polym Sci 37:907–974. https://doi.org/10.1016/j.progpolymsci.2012.02.005
8. Fang J, Kita H, Okamoto K (2000) Hyperbranched polyimides for gas separation applications. 1. Synthesis and characterization. Macromolecules 33:4639–4646. https://doi.org/10.1021/ma9921293
9. He J, Horie K, Yokota R, He F (2001) Preparation of end-crosslinked polyimide gels with high moduli. Polymer 42:4063–4072. https://doi.org/10.1016/S0032-3861(00)00803-X
10. Kawaguchi K, Saito H, Furukawa H, Horie K (2007) Superior nanoporous polyimides via supercritical CO_2 drying of jungle-gym-type polyimide gels. Macromol Rapid Commun 28:96–100. https://doi.org/10.1002/marc.200600587
11. Chidambareswarapattar C, Larimore Z, Sotiriou-Leventis C, Mang JT, Leventis N (2010) One-step room-temperature synthesis of fibrous polyimide aerogels from anhydrides and isocyanates and conversion to isomorphic carbons. J Mater Chem 20:9666–9678. https://doi.org/10.1039/C0JM01844A
12. Leventis N, Sotiriou-Leventis C, Mohite DP, Larimore ZJ, Mang JT, Churu G, Lu H (2011) Polyimide aerogels by ring-opening metathesis polymerization (ROMP). Chem Mater 23:2250–2261. https://doi.org/10.1021/cm200323e
13. Guo H, Meador MAB, McCorkle L, Quade DJ, Guo J, Hamilton B, Cakmak M, Sprowl G (2011) Polyimide aerogels cross-linked through amine functionalized polyoligomeric silsesquioxane. ACS Appl Mater Interfaces 3:546–552. https://doi.org/10.1021/am101123h

14. Guo H, Meador MAB, McCorkle, Quade DJ, Guo J, Hamilton B, Cakmak M (2012) Tailoring properties of cross-linked polyimide aerogels for better Moisture resistance, flexibility, and strength. ACS Appl Mater Interfaces 4:5422–5429. https://doi.org/10.1021/am301347a
15. Chidambareswarapattar C, Xu L, Sotiriou-Leventis C, Leventis N (2013) Robust monolithic multiscale nanoporous polyimides and conversion to isomorphic carbons. RSC Adv 3:26459–26469. https://doi.org/10.1039/C3RA43717E
16. Pei X, Zhai W, Zheng W (2014) Preparation and characterization of highly cross-linked polyimide aerogels based on polyimide containing trimethoxysilane side groups. Langmuir 30:13375–13383. https://doi.org/10.1021/la5026735
17. Meador MAB, Alemán CR, Hanson K, Ramirez N, Vivod SL, Wilmoth N, McCorkle L (2015) Polyimide aerogels with amide cross-links: A low cost alternative for mechanically strong polymer aerogels. ACS Appl Mater Interfaces 7:1240–1249. https://doi.org/10.1021/am507268c
18. Nguyen BN, Cudjoe E, Douglas A, Scheiman D, McCorkle L, Meador MAB, Rowan SJ (2016) Polyimide cellulose nanocrystal composite aerogels. Macromolecules 46:1692–1703. https://doi.org/10.1021/acs.macromol.5b01573
19. Feng J, Wang X, Jiang Y, Du D, Feng J (2016) Study on thermal conductivities of aromatic polyimide aerogels. ACS Appl Mater Interfaces 8:12992–12996. https://doi.org/10.1021/acsami.6b02183
20. Viggiano RP, Williams JC, Schiraldi DA, Meador MAB (2017) Effect of bulky substituents in the polymer backbone on the properties of polyimide aerogels. ACS Appl Mater Interfaces 8:12992–12996. https://doi.org/10.1021/acsami.6b15440
21. Nguyen BN, Meador MAB, Sheiman D, McCorkle (2017) Polyimide aerogels using triisocyanate as cross-linker. ACS Appl Mater Interfaces 9:27313–27321. https://doi.org/10.1021/acsami.7b07821
22. Zhai C, Jana SC (2017) Tuning porous networks in polyimide aerogels for airborne nanoparticle filtration. ACS Appl Mater Interfaces 9:27313–27321. https://doi.org/10.1021/acsami.7b09345
23. Teo N, Jana SC (2018) Solvent effects on tuning pore structures in polyimide aerogels. Langmuir 34:8581–8590. https://doi.org/10.1021/acs.langmuir.8b01513
24. Teo N, Gu Z, Jana SC (2018) Polyimide-based aerogel foams, via emulsion-templating. Polymer 157:95–102. https://doi.org/10.1016/j.polymer.2018.10.030
25. Fan W, Zhang X, Zhang Y, Zhang Y, Liu T (2019) Lightweight, strong, and super-thermal insulating polyimide composite aerogels under high temperature. Comp Sci Technol 173:47–52. https://doi.org/10.1016/j.compscitech.2019.01.025
26. Koebel M, Rigacci A, Achard P (2012) J Sol–Gel Sci Technol 63:315–339. https://doi.org/10.1007/s10971-012-2792-9
27. Cuce E, Cuce PM, Wood CJ, Riffat SB (2014) Toward aerogel based thermal superinsultion in buildings: A comprehensive review. Renew Sus Energy Rev 34:273–299. https://doi.org/10.1016/j.rser.2014.03.017
28. Itatani H (2007) Crosslinked polyimide, composition comprising the same and method for producing the same. US Patent No. US20070106056.
29. Hasegawa G, Shimizu T, Kanamori K, Maeno A, Kaji H, Nakanishi K (2017) Highly flexible hybrid polymer aerogels and xerogels based on resorcinol-formaldehyde with enhanced elastic stiffness and recoverability: Insights into the origin of their mechanical properties. Chem Mater 29:2122–2134. https://doi.org/10.1021/acs.chemmater.6b04706
30. Kanamori K, Nakanishi K, Hanada T (2006) Rigid macroporous poly(divinylbenzene) monoliths with a well-defined bicontinuous morphology prepared by living radical polymerization. Adv Mater 18:2407–2411. https://doi.org/10.1002/adma.200601026
31. Kanamori K, Hasegawa J, Nakanishi K, Hanada T (2008) Facile synthesis of macroporous crosslinked methacrylate gels by atom transfer radical polymerization. Macromolecules 41:7186–7193. https://doi.org/10.1021/ma800563p
32. Hasegawa J, Kanamori K, Nakanishi K, Hanada T, Yamago S (2009) Pore formation in poly(divinylbenzene) networks derived from organotellurium-mediated living radical polymerization. Macromolecules 42:1270–1277. https://doi.org/10.1021/ma802343a
33. Hasegawa J, Kanamori K, Nakanishi K, Hanada T, Yamago S (2009) Rigid cross-linked polyacrylamide monoliths with well-defined macropores synthesized by living polymerization. Macromol Rapid Commun 30:986–990. https://doi.org/10.1002/marc.200900066
34. Hasegawa G, Kanamori K, Nakanishi K, Yamago S (2011) Fabrication of highly crosslinked methacrylate-based polymer monoliths with well-defined macropores via living radical polymerization. Polymer 52:4644–4647. https://doi.org/10.1016/j.polymer.2011.08.028
35. Hasegawa G, Kanamori K, Ishizuka N, Nakanishi K (2012) New monolithic capillary columns with well-defined macropores based on poly(styrene-*co*-divinylbenzene). ACS Appl Mater Interfaces 4:2343–2347. https://doi.org/10.1021/am300552q
36. Dine-Hart RA, Wright WW (1967) Preparation and fabrication of aromatic polyimides. J Appl Polym Sci 11:609–627. https://doi.org/10.1002/app.1967.070110501
37. Koton MM, Meleshko TK, Kudryavtsev VV, Nechayev PP, Kamzolkina YV, Bogorad NN (1982) Investigation of the kinetics of chemical imidization. Polym Sci USSR 24:791–800. https://doi.org/10.1016/0032-3950(82)90334-3
38. Kailani M, Sung CSP (1998) Chemical imidization study by spectroscopic techniques. 2. Polyamic acids. Macromolecules 31:5779–5874. https://doi.org/10.1021/ma9800966
39. Shin TJ, Ree M (2007) Thermal imidization and structural evolution of thin films of poly(4,4'-oxydiphenylene *p*-pyromellitamic diethyl ester). J Phys Chem B 111:13894–13900. https://doi.org/10.1021/jp075067o
40. Ishida H, Wellinghoff ST, Baer E, Koenig JL (1980) Spectroscopic studies of Poly[N,N'-bis(phenoxyphenyl)pyromellitimide]. 1. Structures of the polyimide and three model compounds Macromolecules 13:826–834 https://doi.org/10.1021/ma60076a011
41. Zhang S, Li Y, Yin D, Wang X, Zhao X, Shao Y, Yang S (2005) Study on synthesis and characterization of novel polyimides derived from 2,6-bis(3-aminobenzoyl) pyridine. Eur Polym J 41:1097–1107. https://doi.org/10.1016/j.eurpolymj.2004.11.014
42. Kazaryan LG, Tsvankin DY, Ginzburg BM, Tuichiev S, Korzhavin LN, Frenkel SY (1972) X-ray diffraction study of the crystalline structure of aromatic polyimides. Polym Sci USSR 14:1344–1354. https://doi.org/10.1016/0032-3950(72)90183-9
43. Takahashi N, Yoon DY, Parrish W (1984) Molecular order in condensed states of semiflexible poly(amic acid) and polyimide. Macromolecules 17:2583–2588. https://doi.org/10.1021/ma00142a021
44. Factor BJ, Russell TP, Toney MF (1991) Surface-induced ordering of an aromatic polyimide. Phys Rev Lett 66:1181–1184. https://doi.org/10.1103/PhysRevLett.66.1181
45. Factor BJ, Russell TP, Toney MF (1993) Grazing incidence X-ray scattering studies of thin films of an aromatic polyimide. Macromolecules 26:2847–2859. https://doi.org/10.1021/ma00063a033
46. Ojeda JR, Mobley J, Martin DC (1995) Physical and chemical evolution of PMDA-ODA during thermal imidization. J Polym Sci: Part B 32:559–569. https://doi.org/10.1002/polb.1995.090330404